FASTENER SPACING STUDY OF COLD-FORMED STEEL WALL STUDS USING FINITE STRIP AND FINITE ELEMENT METHODS

RESEARCH REPORT

Brian Post

Dept. of Civil Engineering
Johns Hopkins University
December 2012

1.0 INTRODUCTION

This study aims to compare the finite element and finite strip methods as they are used to perform buckling analyses of cold-formed steel wall studs. Load-bearing cold-formed steel studs are becoming more common as a building material in both commercial and residential structures. Current design methods allow for the determination of the capacity of single studs under compression. However, entire wall systems often have sheathing attached, which adds bracing and increases stability. Examples of sheathing materials include oriented-strand board (OSB), gypsum, and plywood. Recent work by Vieira (2011) has led to the development of a method to calculate the contributions of sheathing and fasteners to overall wall strength. The equations use various parameters of a wall system and calculate spring stiffness values that can be applied to the fasteners along a stud for three degrees-of-freedom: in the plane of the board (k_x), out of the plane of the board (k_y), and rotational (k_ϕ).

In many commercial finite element programs such as ABAQUS, fasteners may be simulated as discrete springs running across the length of a stud with assigned stiffness values. However, the Direct Strength Method, which is a common design technique for cold-formed steel studs, relies on the finite strip method (e.g. CUFSM). Unlike the finite element method, the finite strip method discretizes the member into longitudinal strips and determines the global, local, and distortional buckling modes by forming a signature curve. This method is only dependent on the dimensions of the member's cross-section rather than its longitudinal properties; thus the fasteners must be analyzed as springs smeared across the entire length.

Theoretically, this smeared spring assumption is at its most accurate when the fasteners are closely spaced. The farther apart the fasteners are spaced along the length of a member, the more the results between a finite element and finite strip analysis should diverge. This study attempts to investigate this phenomenon by performing parametric analyses of two different cold-formed steel sections with varying fastener spacing.

2.0 BACKGROUD

2.1 Results of AISI Survey for Parametric Study

The two cold-formed steel sections used for this study were a 362S162-68 and a 600S162-54 (SSMA 2001). The 362S162-68 was chosen because it was the section used by Vieira (2011) and the results could be directly compared. All of the same parameters were used

as Vieira (2011) to assure that the assumptions in the finite strip and finite element models were as accurate as possible. The 600S162-54 was chosen based on a survey taken among professionals from the industry of the typical parameters of a sheathed wall system. The survey asked for the most common stud thicknesses, wall heights, stud spacing, and sheathing/fastener combinations. The results were as follows: 54-mil stud thickness, 10-foot wall height, 16-inch stud spacing, and 7/16-inch-thick OSB with #8 fasteners. Appendix A provides the full results of the survey.

2.2 Spring Stiffness Calculations

The spring stiffness values used in this analysis were obtained using the design equations derived by Vieira (2011). Figure 1 shows a typical cold-formed steel stud wall. The studs are oriented vertically and attached to tracks at the top and bottom. The fasteners to be considered for this analysis include only those attaching sheathing to the field studs. Sheathing can be attached to one side of the wall or both. For this analysis, it is assumed that sheathing is attached to both.

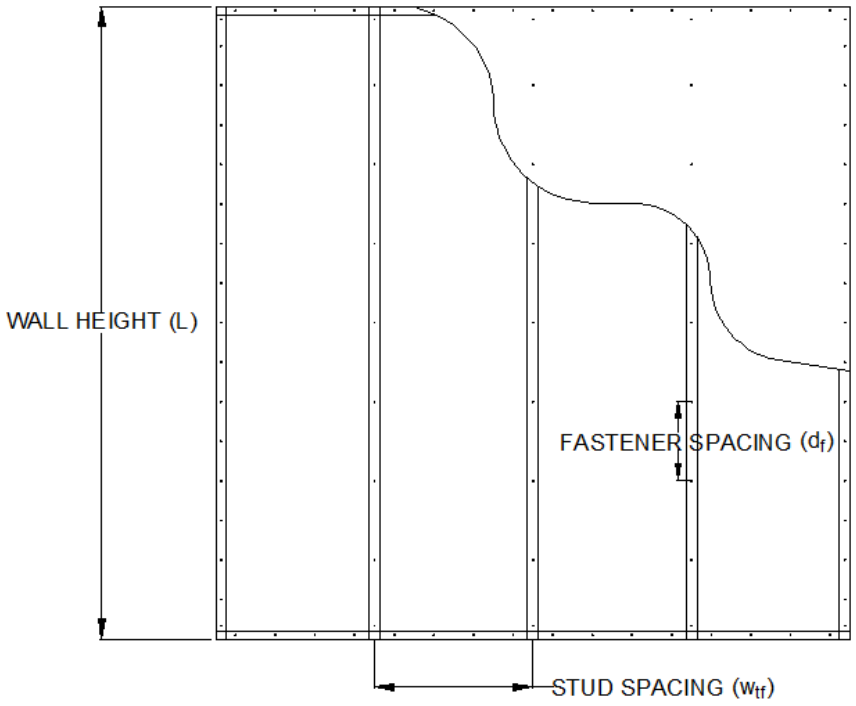

Figure 1 Cold-formed steel stud wall diagram.

Because the sheathing is attached to the flanges of each stud, the fasteners provide restraint. This is represented by springs in three degrees-of-freedom: in the plane of the board (k_x), out of plane of the board (k_y), and rotational (k_ϕ). This is depicted in Figure 2.

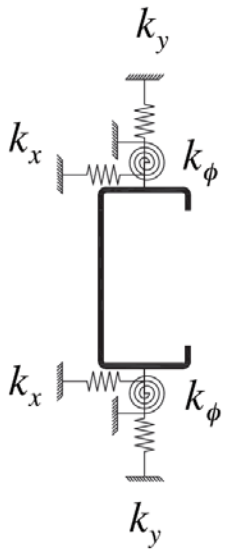

Figure 2 Schematic of cold-formed steel stud with springs representing the stiffness provided by the fasteners (Vieira 2011).

In-plane stiffness provides restraint against the flange translating relative to the sheathing and fastener. This is important for resisting weak-axis flexural buckling and torsion. The total in-plane stiffness is derived from the local stiffness ($k_{x\ell}$) which occurs at the fastener location, and the diaphragm stiffness (k_{xd}) of the entire sheathing (Vieira 2011). Out-of-plane stiffness provides restraint against strong-axis bending perpendicular to the sheathing and contributes to a member's stability in flexural-torsional buckling (Vieira 2011). Rotational stiffness provides restraint against rotation of the flange resulting from any tilting of the fastener or deformation of the sheathing (Vieira 2011). The total rotational stiffness includes both the stiffness provided by the sheathing, $k_{\phi w}$, and the connection stiffness, $k_{\phi c}$ (Vieira 2011). This is important for resisting distortional buckling and contributes to torsional resistance.

Vieira (2011) provides an exact and simplified equation for calculating k_{xd}. Likewise, $k_{x\ell}$ can either be calculated analytically or determined from testing. Because this study is for design purposes, the simplified and analytical approaches were used to determine k_{xd} and $k_{x\ell}$,

respectively. Also, k_ϕ can be determined from tests, but the semi-empirical equations from Vieira (2011) were used.

The simplified equation for k_{xd} and the analytical equation for $k_{x\ell}$ are as follows:

$$k_{xd} = \frac{\pi^2 G t_{board} d_f w_{tf}}{L^2} \tag{1}$$

where:

G = shear stiffness of the sheathing (ksi)

t_{board} = thickness of the sheathing (in)

d_f = fastener spacing (in)

w_{tf} = stud spacing/tributary width of fastener (in)

L = height of sheathing/length of member (in)

Likewise, the equation for $k_{x\ell}$ is:

$$k_{x\ell} = \frac{3Ed^4 t^3 \pi}{4t_{board}^2 (9d^4\pi + 16 t_{board} t^3)} \tag{2}$$

where:

E = Young's modulus for cold-formed steel (ksi)

d = diameter of fastener (in)

t = stud thickness (in)

t_{board} = thickness of sheathing (in)

From the local and diaphragm stiffness values, the overall in-plane stiffness for discrete and smeared conditions, respectively, is calculated as follows:

$$k_x = \left(\frac{1}{k_{x\ell}} + \frac{1}{k_{xd}} \right)^{-1} \tag{3}$$

$$\underline{k}_x = \frac{k_x}{d_f} \tag{4}$$

The out-of-plane stiffness k_y is calculated from:

$$k_y = \frac{(EI)_{w-parallel} \pi^4 d_f}{L^4} \tag{5}$$

$$\underline{k}_y = \frac{k_y}{d_f} \tag{6}$$

where:

$(EI)_{w\text{-parallel}}$ = sheathing rigidity based on the stress parallel to the strength axis (k-in^2/ft)

d_f = fastener spacing (in)

L = height of sheathing/length of member (in)

The equations for rotational stiffness are as follows:

$$\underline{k}_{\phi c} = 0.000035Et^2 + 75 \tag{7}$$

$$\underline{k}_{\phi w} = \frac{(EI)_{w-perpendicular}}{d_f} \tag{8}$$

$$\underline{k}_{\phi} = \frac{1}{\left(\frac{1}{\underline{k}_{\phi c}} + \frac{1}{\underline{k}_{\phi w}}\right)} \tag{9}$$

$$k_{\phi} = \underline{k}_{\phi} d_f \tag{10}$$

where:

E = Young's modulus for cold-formed steel (psi)

t = stud thickness (in)

$(EI)_{w\text{-perpendicular}}$ = sheathing rigidity based on the stress perpendicular to the strength axis (lb-in^2/in)

d_f = fastener spacing (in)

It should be noted that in equation (7), E is in units of psi and t is in units of inches. In equation (8), $(EI)_{w\text{-perpendicular}}$ is in units of lb·in^2/in. Equation (9) gives the rotational stiffness in units of kips·in/in/rad. This is the smeared stiffness that must be applied to springs in CUFSM. To obtain the stiffness for discrete springs, the result is multiplied by d_f to give the stiffness in units of kips·in/rad (equation 10). However, equations (3) and (5) give k_x and k_y in units of kips/in. These values must be divided by d_f to give the values for smeared springs, $\underline{k}_x$ and $\underline{k}_y$, in units of kips/in/in. This is expressed in equations (4) and (6), respectively.

3.0 ANALYSIS of 362S162-68

Vieira (2011) provides a thorough design example using CUFSM with spring stiffness values calculated from the equations. An example is also provided in Appendix B of this report. The parameters include a 96-inch-long 362S162-68 section, 7/16-inch-thick OSB sheathing, and #8 fasteners spaced at 12 inches along the length of the member with tributary width (stud

spacing) of 24 inches. The procedure for analyzing the member in CUFSM provided by Vieira (2011) was closely followed, with the exception of the use of the constrained finite strip method (cFSM), which was not used for analyzing members with fixed boundary conditions in this study.

3.1 CUFSM Models

The first step was to create a CUFSM model of a 96-inch-long 362S162-68 section. The latest version of CUFSM (version 4.03) was used, which allows for the implementation of general boundary conditions in addition to the traditional signature curve analysis. It should be noted that all models used out-to-out dimensions rather than centerline dimensions. In addition, rounded corners were neglected. All geometric dimensions for the section were obtained from the AISI Cold-Formed Steel Design Manual. Both the actual dimensions and simplified model dimensions are illustrated in Figure 3. The cross-sectional area of the member is 0.524 in^2 and the design thickness is 0.0713 in.

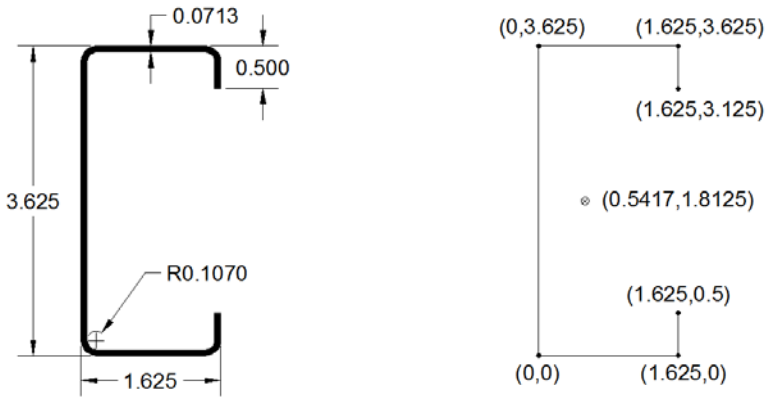

(a) (b)

Figure 3 (a) Actual dimensions and (b) simplified dimensions of 362S162-68 section.

3.1.1 Signature Curve (Simply-Supported Boundary Conditions)

Figure 4 shows the input window for the 362S162-68 model without springs. A yield strength, F_y of 50 ksi was assumed, which resulted in a squash load, P_y of 28.0744 kips. To begin, a signature curve was created under the assumption of "simple-simple (S-S)" boundary conditions. Figure 5 shows the resulting signature curve.

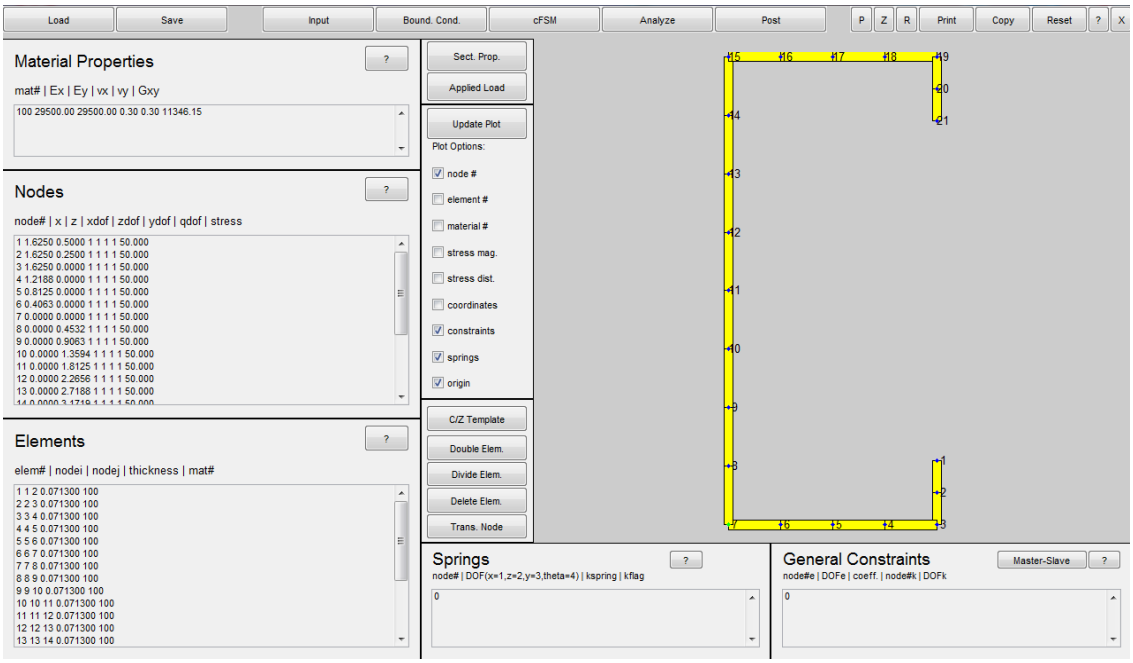

Figure 4 CUFSM input window for 362S162-68 section.

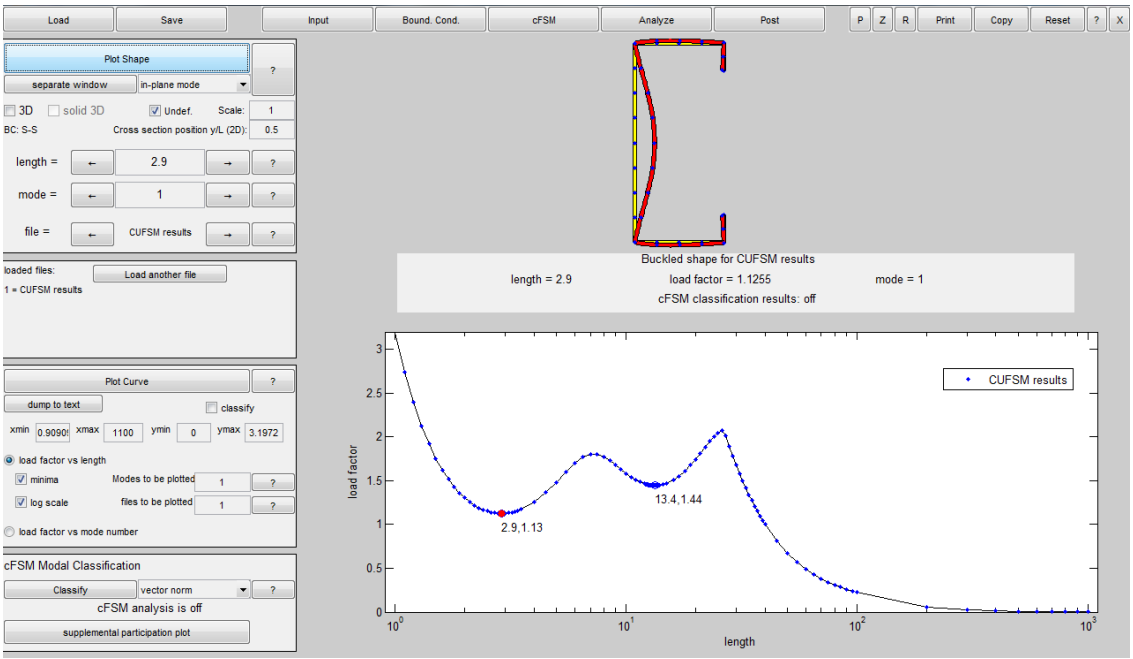

Figure 5 Signature curve for 362S162-68 section.

The first and second minima from left to right represent the local and distortional buckling modes, respectively. To obtain the critical loads, the load factor corresponding to each minimum is multiplied by P_y. The critical load for global buckling is found by obtaining the load

factor corresponding to the length of the member, which in this case is 96 inches, and multiplying that by P_y.

3.1.2 General Boundary Conditions (Fixed-Fixed)

Determining critical loads using the signature curve only works for simply-supported boundary conditions. For fixed-fixed (clamped-clamped) boundary conditions, the analysis more closely resembles the finite element method, where multiple eigenvalues representing the different buckling modes are evaluated and the critical modes are chosen. For this analysis, 20 eigenvalues were evaluated over the 96-inch length. The output is shown in Figure 6. CUFSM provides a colorful plot that classifies each mode into its respective buckling types. The goal is to find the modes that most closely resemble pure local, pure distortional, and pure global buckling.

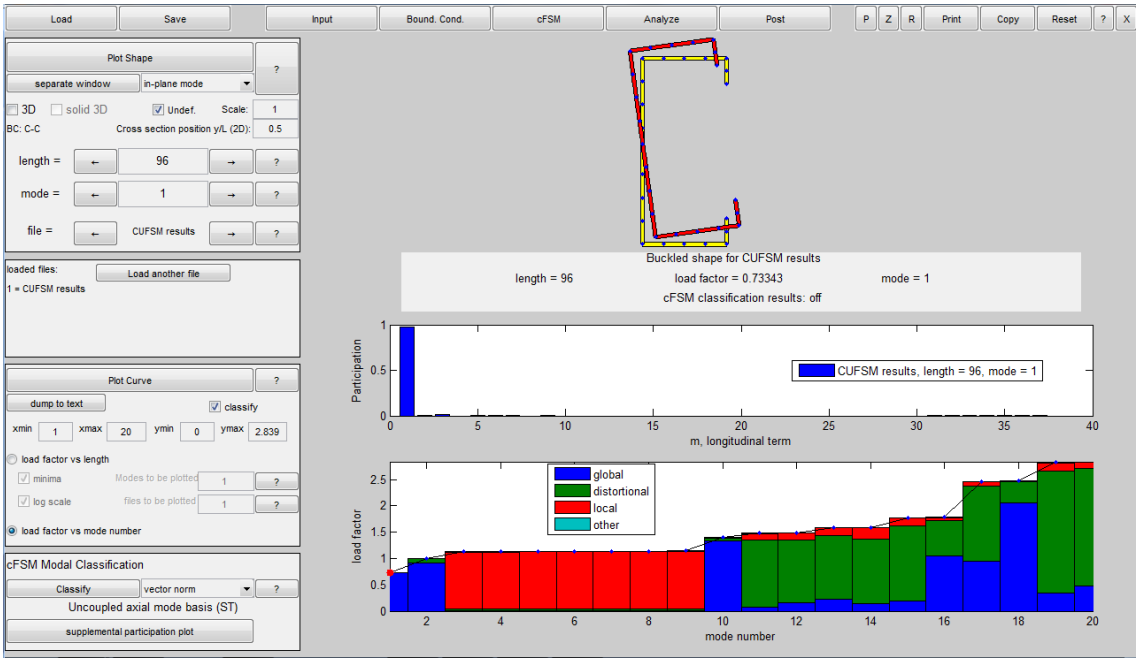

Figure 6 CUFSM post-processing window for general boundary condition analysis of 362S162-68 section.

It should be noted that CUFSM also provides the option of using the constrained finite strip method (cFSM), which isolates each buckling mode and evaluates them separately. This was the method used by Vieira (2011). However, the load factors are often higher than those obtained if all buckling modes are analyzed together and thus was not used in this study.

3.1.3 Adding Smeared Springs

Once the initial analysis was complete, smeared springs were then added to the model. Spring stiffness values for all models are listed in Appendix C. Figure 7 shows the input window with springs included, the stiffness values of which correspond to 12-inch fastener spacing. The smeared stiffness values of $\underline{k}_x$, $\underline{k}_y$, and $\underline{k}_\phi$ were simply entered into the "Springs" box for degrees-of-freedom 1, 2, and 4, respectively. The parameters used to calculate $\underline{k}_x$, $\underline{k}_y$, and $\underline{k}_\phi$ were the same as those presented by Vieira (2011) in the design problem:

$G = 190$ ksi

$t_{board} = 7/16$ in

$(EI)_{w\text{-}parallel} = 78$ k·in^2/ft

$(EI)_{w\text{-}perpendicular} = 16$ k·in^2/ft

$w_{tf} = 24$ in

$d = 0.164$ in

The fastener diameter, d was obtained from the AISI code for a #8 fastener, not the value measured by Vieira (2011). Since this was a parametric analysis, the model was run for fasteners spaced at 2 inches, 6 inches, 12 inches, 24 inches, and 48 inches.

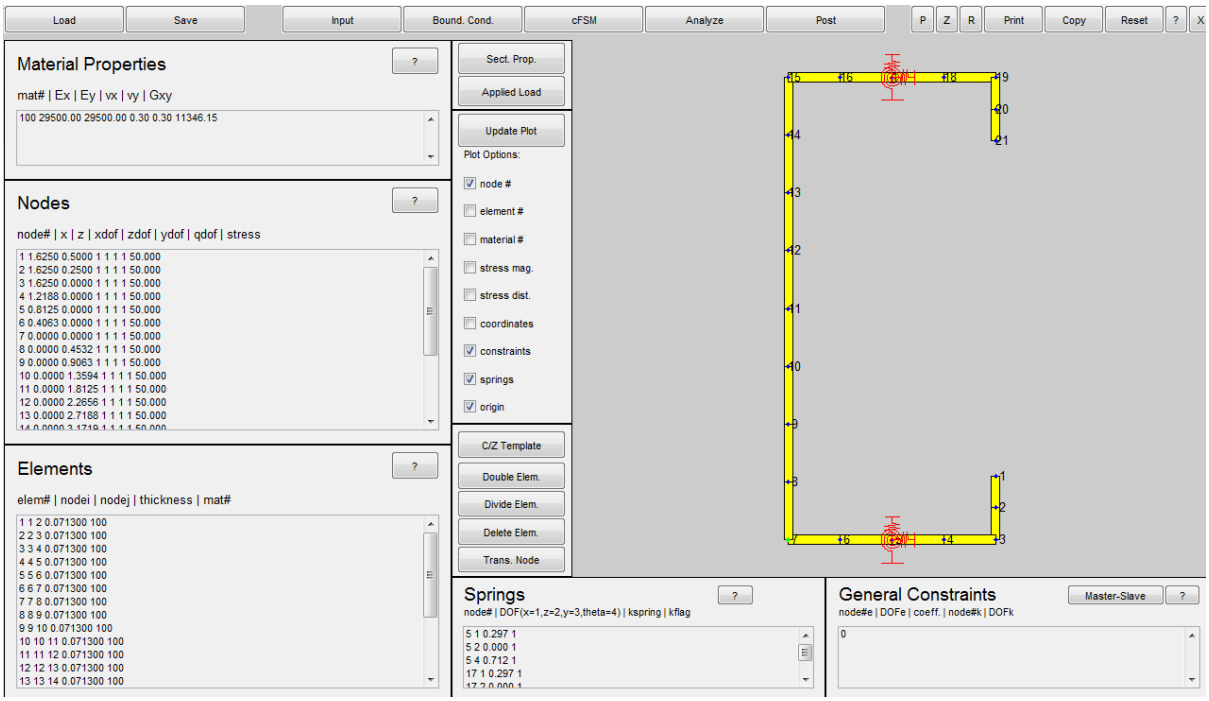

Figure 7 CUFSM input window for 362S162-68 section with smeared springs reflecting 12-inch fastener spacing.

3.2 ABAQUS Models

The other half of this study involved creating finite element models of the member in ABAQUS. A buckling analysis of the shell element model was performed and the local, distortional, and global modes were found from the eigenvalues evaluated. ABAQUS CAE was used for this study, although the input file could also be used to directly create the models.

3.2.1 Methodology to Create Shell Element Models in ABAQUS CAE

For consistency, the same out-to-out dimensions were used for the 362S162-68 member in ABAQUS. The stud was created as a part in the CAE part module where the cross-section was defined and then extruded to create a three-dimensional model. The stud was assigned material properties, which included a Young's modulus of 29,500 ksi and Poisson's ratio of 0.3 (accepted values for cold-formed steel). It was also assigned a thickness of 0.0713 inches consisting of homogeneous shell elements. A buckling step was created in the step module, with 100 eigenvalues requested for analysis. The part was meshed using S4R shell elements and a seed size of 0.25 inches. A close-up of the meshing as seen through the CAE can be found in Figure 8. The mesh was defined "by part," which is considered "dependent" in the instance module.

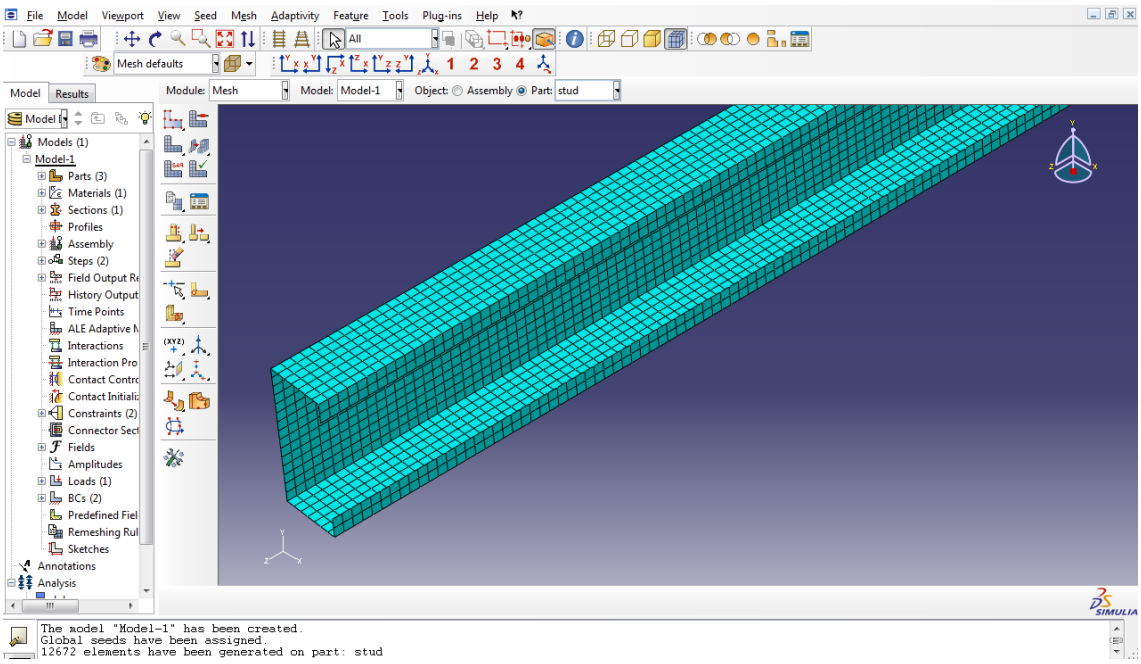

Figure 8 Close-up of meshing pattern as seen in ABAQUS CAE

The most difficult part of creating the ABAQUS model was establishing ideal boundary conditions that closely resembled the assumptions of CUFSM. For fixed-fixed boundary conditions, a reference point was created at each end of the cross-section and all of the nodes on the cross-section were tied to this point using a multipoint constraint (MPC) in the interaction module. This is shown in Figure 9. It was assumed that this reference point was located at the centroid of the cross-section, and not the shear center. All loads and boundary conditions were then applied to this reference point, which acted as a master node. A compressive unit load was applied at one end. This end was fixed for all degrees-of-freedom except longitudinal translation (U3). The other unloaded end was fully fixed.

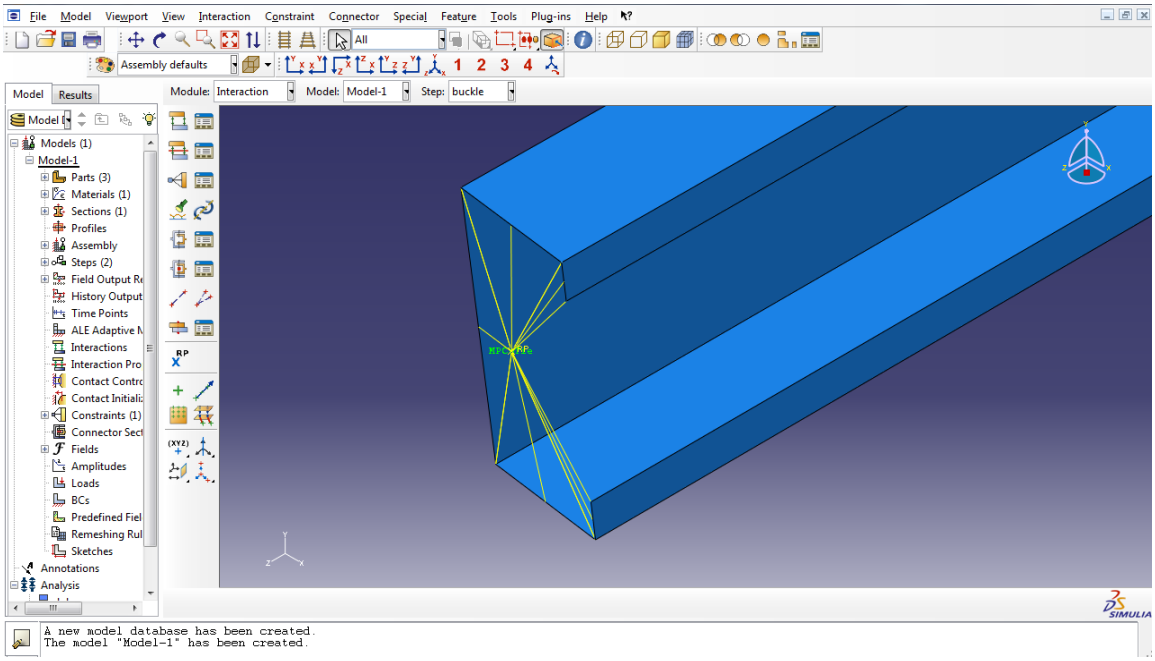

Figure 9 Cross-sectional end nodes tied to master node at centroid using MPC Tie.

For simply-supported boundary conditions, MPC ties were not used. Rather, a shell edge load was applied around the perimeter of the cross-section. To assure that the load was equivalent to a unit load, the inverse of the perimeter length was calculated. For example, the perimeter of a 362S162-68 is the sum of the web, flange, and lip lengths, or $3.625 + 2 \times 1.625 + 2 \times 0.5 = 7.875$ inches. The inverse of this gives a unit load of $1/7.875 = 0.1270$ kips/inch. Unlike the fixed condition, this load was applied at both ends. Likewise, both ends were set as rollers, allowing for rotation and longitudinal translation (constraining the U1, U2, and UR3

degrees of freedom). This is shown in Figure 10. To assure that the member was static, longitudinal translation (U3) was constrained at the center of the member. This was achieved by partitioning the member at the center and applying the constraint, which is shown in Figure 11.

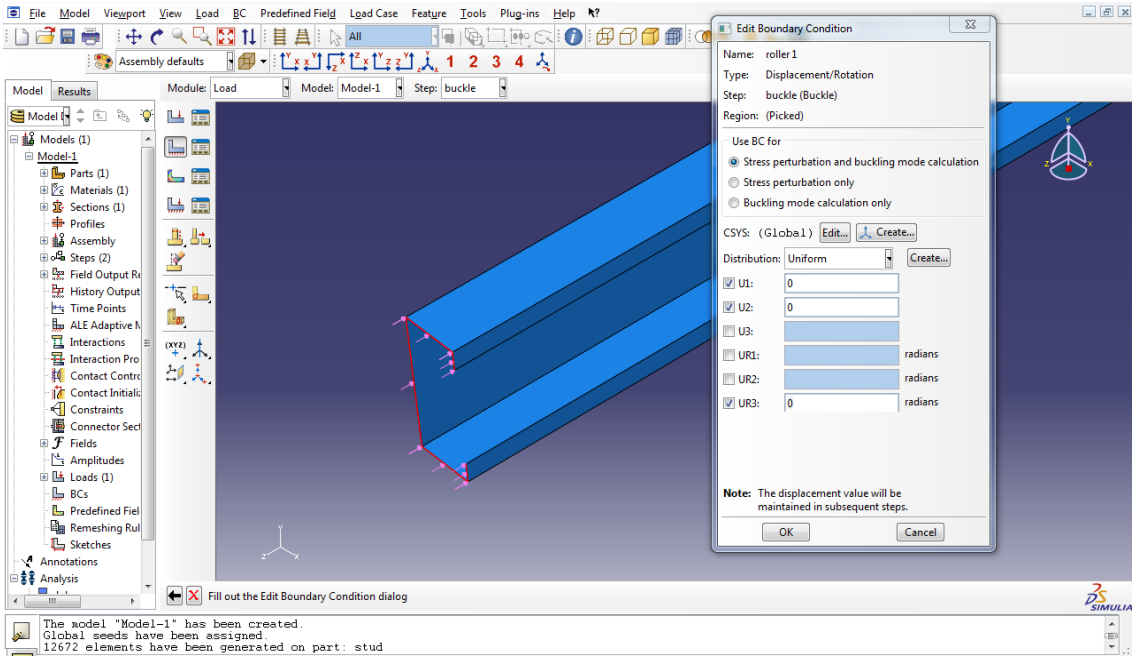

Figure 10 Load and boundary conditions applied around perimeter of cross-section for simply-supported boundary conditions.

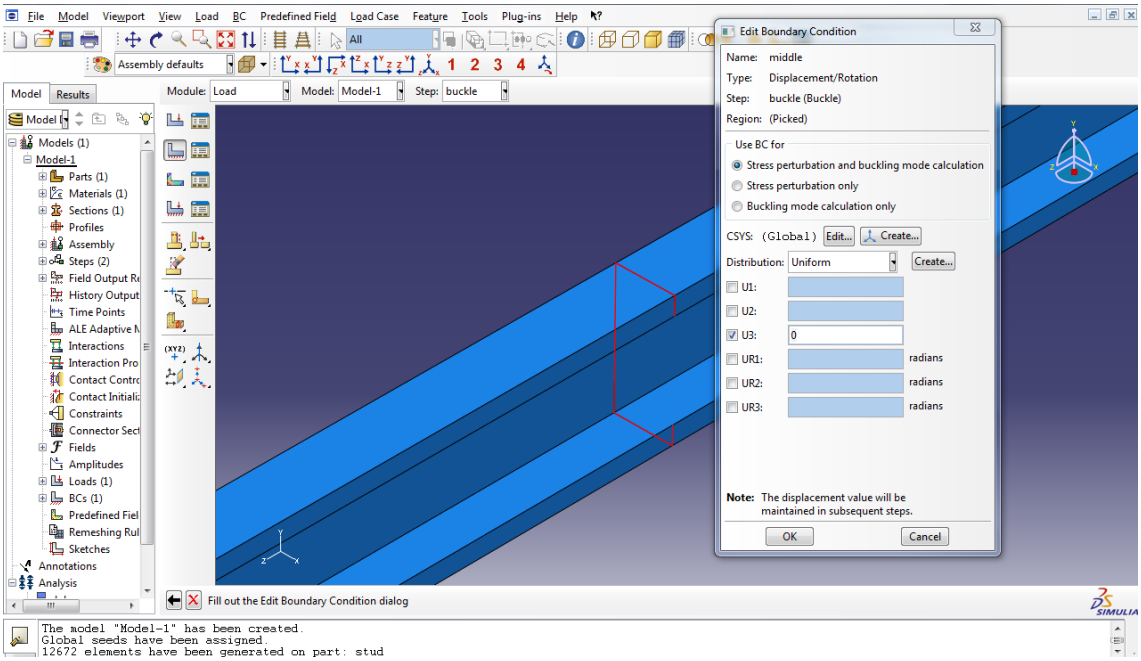

Figure 11 Longitudinal translation (U3) constrained at the center of the member.

3.2.2 Adding Discrete Springs

Once the model was created and run for both simply-supported and fixed-fixed boundary conditions, discrete springs were added along the length of the member. This was done by partitioning the flanges of the stud to create discrete points at the desired fastener locations. These points were then assigned stiffness values by classifying them as springs connected to the ground. The discrete stiffness values for k_x, k_y, and k_ϕ were entered for degrees-of-freedom 1, 2, and 4, respectively. It should be noted that degrees-of-freedom 3, 5, and 6 were assumed to have stiffness values of zero in ABAQUS. Tables of all stiffness values used in both CUFSM and ABAQUS can be found in Appendix C. The stud with discrete springs spaced at 12 inches is shown in Figure 12. In addition to the 12-inch spacing, springs were also placed 2 inches from the ends to account for connections to track members. This was the case for all models.

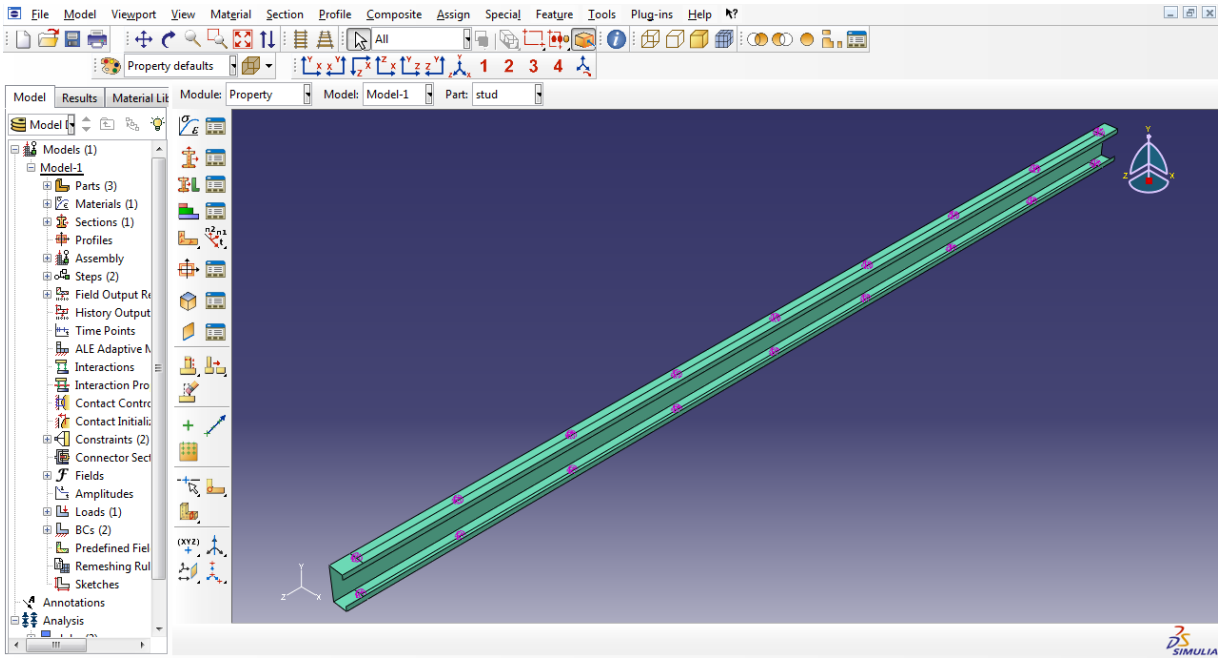

Figure 12 Model with discrete springs.

3.3 Results

The critical loads for the local, distortional, and global buckling modes were found using both CUFSM and ABAQUS for 2-inch, 6-inch, 12-inch, 24-inch, and 48-inch fastener spacing, in addition to the model without springs. The results are presented in Table 1 for simply-supported boundary conditions and Table 2 for fixed-fixed boundary conditions. The percent differences listed are expressed relative to the CUFSM result for each case.

Table 1 Comparison of CUFSM and ABAQUS for 362S162-68 with simply-supported boundary conditions.

NO SPRINGS			
Buckling Mode	**CUFSM P_{cr} (kips)**	**ABAQUS P_{cr} (kips)**	**% Difference**
Local	31.598	31.728	0.41%
Distortional	40.539	39.109	3.53%
Global	6.6882	6.6160	1.07%
2-inch spring spacing			
Buckling Mode	**CUFSM P_{cr} (kips)**	**ABAQUS P_{cr} (kips)**	**% Difference**
Local	31.601	31.753	0.48%
Distortional	45.014	40.659	9.67%
Global	37.263	37.731	1.26%
6-inch spring spacing			
Buckling Mode	**CUFSM P_{cr} (kips)**	**ABAQUS P_{cr} (kips)**	**% Difference**
Local	31.601	31.747	0.46%
Distortional	43.768	39.987	8.64%
Global	36.895	37.282	1.05%
12-inch spring spacing			
Buckling Mode	**CUFSM P_{cr} (kips)**	**ABAQUS P_{cr} (kips)**	**% Difference**
Local	31.601	31.744	0.45%
Distortional	42.861	39.627	7.55%
Global	36.342	36.631	0.80%
24-inch spring spacing			
Buckling Mode	**CUFSM P_{cr} (kips)**	**ABAQUS P_{cr} (kips)**	**% Difference**
Local	31.598	31.741	0.45%
Distortional	42.069	39.190	6.84%
Global	35.256	35.294	0.11%
48-inch spring spacing			
Buckling Mode	**CUFSM P_{cr} (kips)**	**ABAQUS P_{cr} (kips)**	**% Difference**
Local	31.598	31.739	0.45%
Distortional	41.443	39.178	5.47%
Global	33.136	29.358	11.40%

Table 2 Comparison of CUFSM and ABAQUS for 362S162-68 with fixed-fixed boundary conditions.

NO SPRINGS			
Buckling Mode	**CUFSM P_{cr} (kips)**	**ABAQUS P_{cr} (kips)**	**% Difference**
Local	31.629	31.713	0.27%
Distortional	41.550	39.795	4.22%
Global	20.591	20.131	2.23%
2-inch spring spacing			
Buckling Mode	**CUFSM P_{cr} (kips)**	**ABAQUS P_{cr} (kips)**	**% Difference**
Local	31.631	31.736	0.33%
Distortional	45.972	41.095	10.61%
Global	115.450	109.45	5.20%
6-inch spring spacing			
Buckling Mode	**CUFSM P_{cr} (kips)**	**ABAQUS P_{cr} (kips)**	**% Difference**
Local	31.631	31.728	0.31%
Distortional	44.739	40.495	9.49%
Global	97.449	94.537	2.99%
12-inch spring spacing			
Buckling Mode	**CUFSM P_{cr} (kips)**	**ABAQUS P_{cr} (kips)**	**% Difference**
Local	31.631	31.725	0.30%
Distortional	43.838	40.426	7.78%
Global	84.639	81.791	3.36%
24-inch spring spacing			
Buckling Mode	**CUFSM P_{cr} (kips)**	**ABAQUS P_{cr} (kips)**	**% Difference**
Local	31.629	31.723	0.30%
Distortional	43.052	39.796	7.56%
Global	72.920	64.515	11.53%
48-inch spring spacing			
Buckling Mode	**CUFSM P_{cr} (kips)**	**ABAQUS P_{cr} (kips)**	**% Difference**
Local	31.629	31.721	0.29%
Distortional	42.437	39.788	6.24%
Global	58.746	38.336	34.74%

It can be seen that springs have a strong influence on global buckling. This is evident from the significant increase in P_{cr} from the models with no springs to the models with springs at 2-inch spacing. As expected, the global results appear to diverge as fastener spacing increases, especially for fixed-fixed boundary conditions. The local values appear to be generally consistent throughout, which is expected as springs typically do not influence local buckling. Also, springs appear to have only a minimal influence on distortional buckling.

4.0 ANALYSIS OF 600S162-54

In addition to the 362S162-68 section, a 600S162-54 section was also analyzed in this study. The choice of this section was based on the results of the survey conducted among professionals from the industry, as discussed in Section 2.1 and provided in Appendix A. The parameter changes in the spring stiffness equations are as follows:

t = 0.0566 in

L = 120 in

w_{tf} = 16 in

The actual and simplified model dimensions are illustrated in Figure 13. In addition, the cross-sectional area of the member is 0.556 in^2 and the design thickness is 0.0566 in.

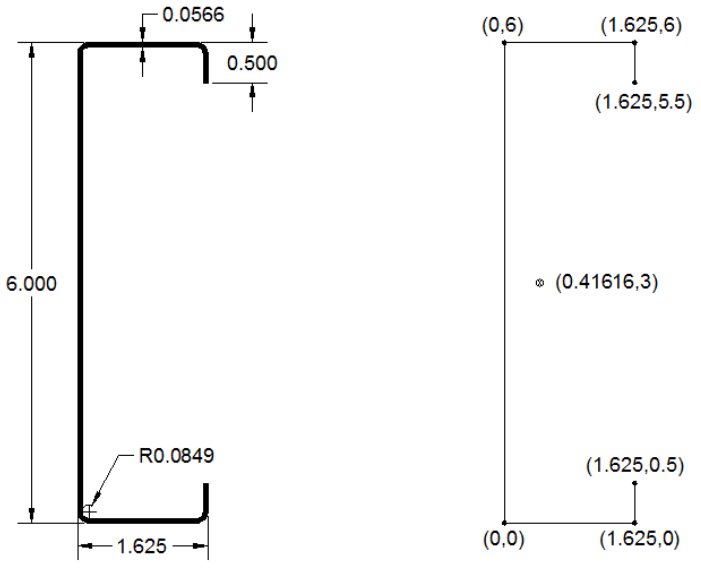

(a) (b)

Figure 13 (a) Actual dimensions and (b) simplified dimensions of 600S162-54 section.

For this section, 2-inch, 6-inch, 12-inch, 24-inch, 40-inch, and 60-inch fastener spacing was analyzed. Unlike the 362S162-68 section, which included 48-inch spacing, 40-inch and 60-inch were chosen for the 600S162-54 since a 120-inch-long stud can be divided into even increments of 40 inches and 60 inches and not 48 inches. The 60-inch spacing was expected to have a similar effect on the 120-inch-long 600S162-54 as the 48-inch spacing had on the 96-inch-long 362S162-68, essentially bisecting it with one fastener in the center and a fastener at each end.

4.1 CUFSM Models

For the 600S162-54 section, the same procedure was used as that for the 362S162-68 section. However, because of the slenderness of the 600S162-54, there was generally no distortional minimum, as seen in Figure 14.

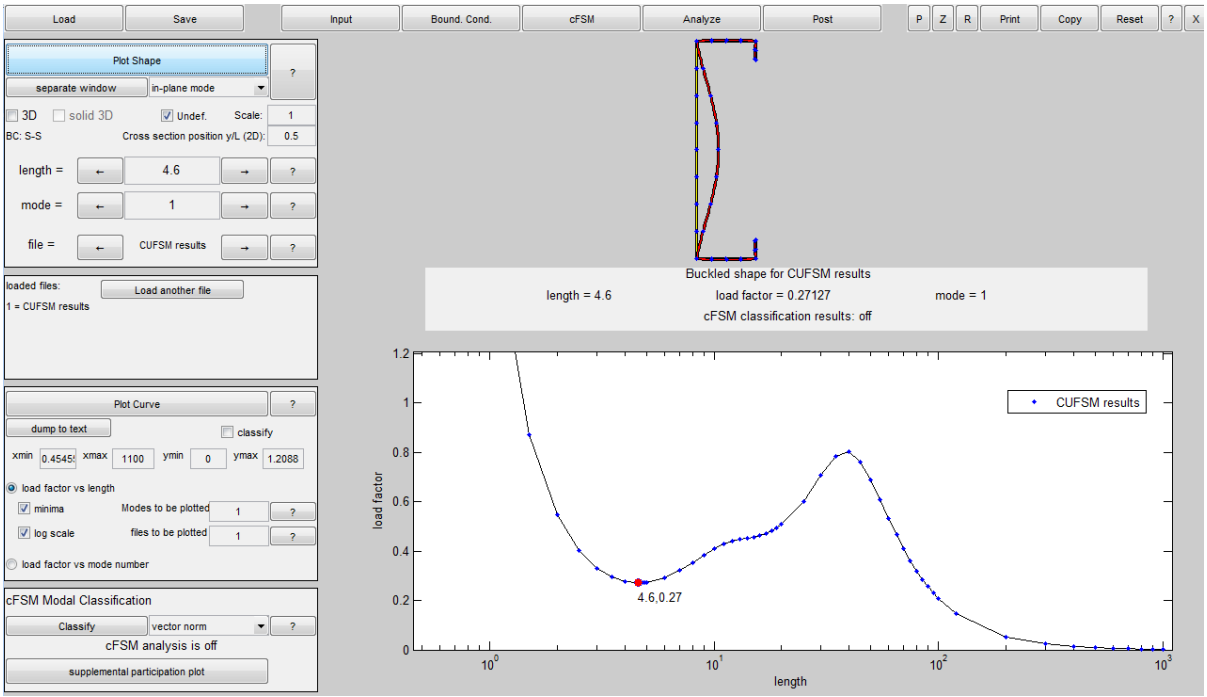

Figure 14 Signature curve for 600S162-54 showing no distinct minimum for distortional buckling.

To determine the critical load for distortional buckling, cFSM was run in conjunction with the signature curve so that the distortional mode was isolated, giving a distinct minimum.

This is shown in Figure 15. The half-wavelength of this minimum was then used in the original signature curve to determine the load factor (Li 2010).

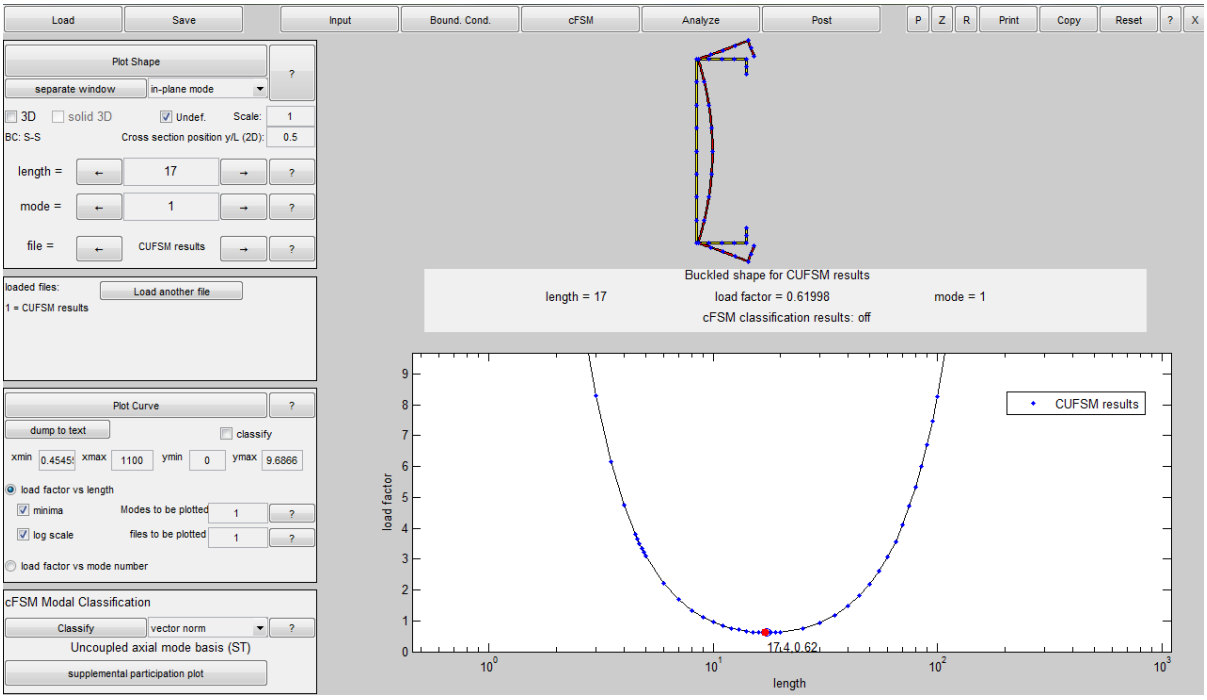

Figure 15 cFSM signature curve analysis for distortional buckling.

The procedure for fixed-fixed boundary conditions remained unchanged with the exception of the number of eigenvalues needed in the solution. Because the 600S162-54 is stronger in flexural and flexural-torsional buckling, more eigenvalues were needed to find a purely global mode.

4.2 ABAQUS Models

The procedure in ABAQUS for a 600S162-54 stud was identical to that for the 362S162-68 stud with the exception of the initial geometric inputs to define the stud part. Also, more eigenvalues were needed in the analysis to account for higher values for global buckling.

4.3 Results

The results of the CUFSM and ABAQUS comparison under simply-supported boundary conditions and fixed-fixed boundary conditions for a 600S162-54 member are summarized in Tables 3 and 4. Again, the percent differences listed are relative to the CUFSM values.

Table 3 Comparison of CUFSM and ABAQUS for 600S162-54 with simply-supported boundary conditions.

NO SPRINGS			
Buckling Mode	**CUFSM P_{cr} (kips)**	**ABAQUS P_{cr} (kips)**	**% Difference**
Local	7.8689	7.8923	0.30%
Distortional	13.794	13.350	3.22%
Global	4.2365	4.216	0.49%
2-inch spring spacing			
Buckling Mode	**CUFSM P_{cr} (kips)**	**ABAQUS P_{cr} (kips)**	**% Difference**
Local	7.8703	7.8969	0.34%
Distortional	15.482	13.922	10.08%
Global	60.759	60.818	0.10%
6-inch spring spacing			
Buckling Mode	**CUFSM P_{cr} (kips)**	**ABAQUS P_{cr} (kips)**	**% Difference**
Local	7.8692	7.8954	0.33%
Distortional	14.879	13.685	8.02%
Global	60.301	60.440	0.23%
12-inch spring spacing			
Buckling Mode	**CUFSM P_{cr} (kips)**	**ABAQUS P_{cr} (kips)**	**% Difference**
Local	7.8692	7.8945	0.32%
Distortional	14.68	13.558	7.64%
Global	59.811	59.879	0.11%
24-inch spring spacing			
Buckling Mode	**CUFSM P_{cr} (kips)**	**ABAQUS P_{cr} (kips)**	**% Difference**
Local	7.8692	7.8936	0.32%
Distortional	14.432	13.424	6.98%
Global	58.772	58.704	0.12%
40-inch spring spacing			
Buckling Mode	**CUFSM P_{cr} (kips)**	**ABAQUS P_{cr} (kips)**	**% Difference**
Local	7.8689	7.8936	0.31%
Distortional	14.248	13.365	6.20%
Global	57.261	40.277	29.66%
60-inch spring spacing			
Buckling Mode	**CUFSM P_{cr} (kips)**	**ABAQUS P_{cr} (kips)**	**% Difference**
Local	7.8689	7.8928	0.30%
Distortional	14.131	13.369	5.39%
Global	55.074	35.046	36.37%

Table 4 Comparison of CUFSM and ABAQUS for 600S162-54 with fixed-fixed boundary conditions.

NO SPRINGS			
Buckling Mode	**CUFSM P_{cr} (kips)**	**ABAQUS P_{cr} (kips)**	**% Difference**
Local	7.8819	7.8892	0.09%
Distortional	13.019	12.821	1.52%
Global	15.522	15.494	0.18%
2-inch spring spacing			
Buckling Mode	**CUFSM P_{cr} (kips)**	**ABAQUS P_{cr} (kips)**	**% Difference**
Local	7.8828	7.8962	0.17%
Distortional	14.296	13.200	7.67%
Global	162.00*	146.08*	9.83%
6-inch spring spacing			
Buckling Mode	**CUFSM P_{cr} (kips)**	**ABAQUS P_{cr} (kips)**	**% Difference**
Local	7.8825	7.894	0.15%
Distortional	13.737	13.106	4.59%
Global	136.33	127.02	6.82%
12-inch spring spacing			
Buckling Mode	**CUFSM P_{cr} (kips)**	**ABAQUS P_{cr} (kips)**	**% Difference**
Local	7.8825	7.8917	0.12%
Distortional	13.564	13.620	0.41%
Global	110.06	104.93	4.66%
24-inch spring spacing			
Buckling Mode	**CUFSM P_{cr} (kips)**	**ABAQUS P_{cr} (kips)**	**% Difference**
Local	7.8822	7.8887	0.08%
Distortional	13.393	13.537	1.08%
Global	98.733	85.055	13.85%
40-inch spring spacing			
Buckling Mode	**CUFSM P_{cr} (kips)**	**ABAQUS P_{cr} (kips)**	**% Difference**
Local	7.8822	7.8831	0.01%
Distortional	13.277	12.795	3.63%
Global	76.765	54.986	28.37%
60-inch spring spacing			
Buckling Mode	**CUFSM P_{cr} (kips)**	**ABAQUS P_{cr} (kips)**	**% Difference**
Local	7.8822	7.8788	0.04%
Distortional	13.207	12.794	3.13%
Global	64.330	36.010	44.02%

*Critical loads for global buckling at 2-inch spring spacing were difficult to determine by visual inspection. Possibly, more eigenvalues are needed to find a more purely global mode.

The results for this section show similar patterns to those for the 362S162-68 section. The critical loads for local buckling show very little variation, regardless of boundary conditions or fastener spacing. The distortional modes were very difficult to determine by visual inspection in ABAQUS. Often there were multiple modes that appeared to be distortional with some local buckling, making it difficult to choose the critical mode. Also, because of the lack of a distinct distortional minimum on the CUFSM signature curve, the method described provided only an approximation of the actual critical distortional buckling load.

It is interesting to note for the simply-supported case that the two models with spring spacing greater than 24 inches had global values significantly different than their corresponding CUFSM values. The global values were very similar for the 2-inch, 6-inch, 12-inch, and 24-inch cases. For the 40-inch and 60-inch cases, there was a buckling mode that closely matched the global buckling magnitude and deformed shape in CUFSM, but there was another global buckling mode at a lower magnitude that served as the critical buckling mode. This is demonstrated in Figures 16 and 17. It is clear from the deformed shapes that the higher buckling mode in ABAQUS, although not the critical mode, more closely resembled the CUFSM result.

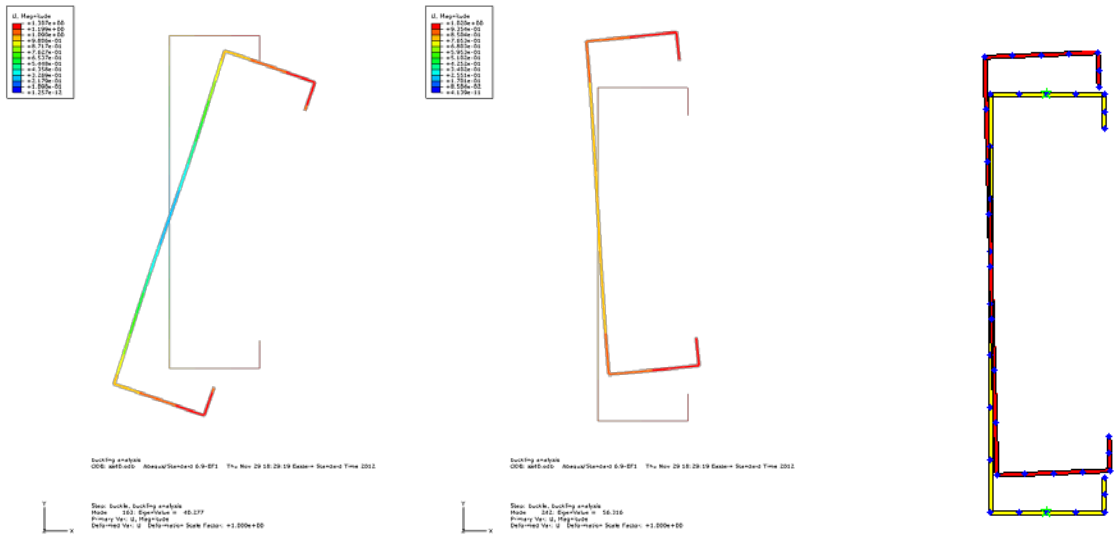

(a) (b) (c)

Figure 16 Comparison of ABAQUS and CUFSM for global buckling of 600S162-54: (a) Deformed shape of critical global buckling mode at eigenvalue 163 in ABAQUS resulting in critical load of 40.277 kips; (b) deformed shape of global buckling mode at eigenvalue 242 in ABAQUS resulting in load of 56.316 kips; (c) deformed shape of global buckling from CUFSM signature curve resulting in critical load of 57.261 kips.

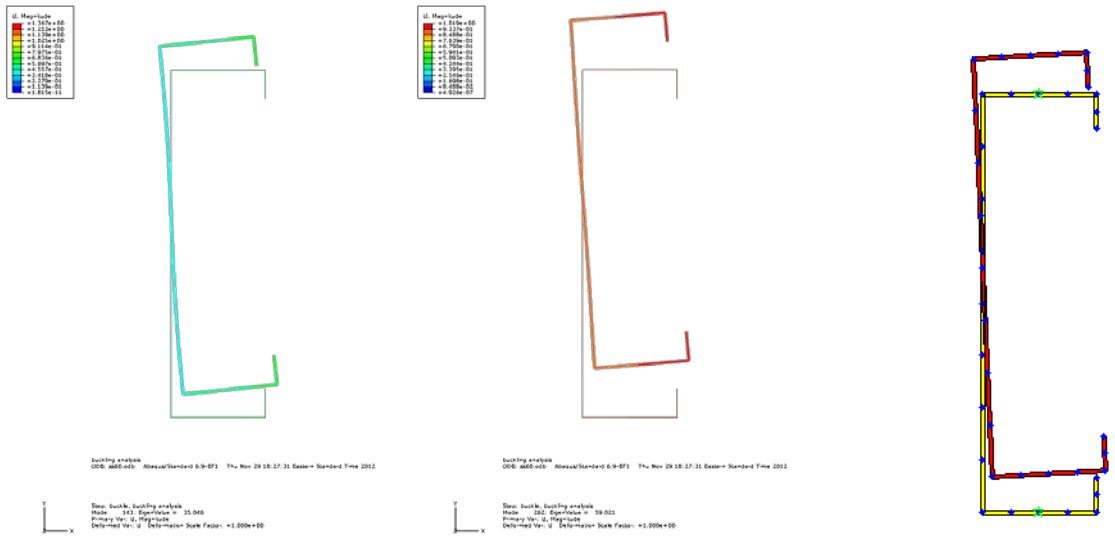

(a) (b) (c)

Figure 17 Comparison of ABAQUS and CUFSM for global buckling of 600S162-54: (a) Deformed shape of critical global buckling mode at eigenvalue 143 in ABAQUS resulting in critical load of 35.046 kips; (b) deformed shape of global buckling mode at eigenvalue 262 in ABAQUS resulting in load of 59.021; (c) deformed shape of global buckling from CUFSM signature curve resulting in critical load of 55.074 kips.

The 40-inch and 60-inch cases with fixed-fixed boundary conditions also exhibited significant divergence between the two models, with the ABAQUS critical global loads consistently being lower. It should be noted that it was difficult to determine the global mode in CUFSM as many lower modes had some global buckling, but not enough to be considered the critical mode.

5.0 COMBINED RESULTS

To develop a better sense of the overall effect of fastener spacing, a comparison of results from the two sections were plotted in three different figures for local, distortional, and global buckling. Figures 18, 19, and 20 provide plots of the ratio of CUFSM critical loads to ABAQUS critical loads against the ratio of spring spacing to member length (d_f/L) for each type of buckling on a logarithmic scale. It should be noted that for global buckling, the results were plotted against d_f/L_{cre}, or d_f/KL, where K is 1.0 for simply-supported boundary conditions and 0.5 for fixed-fixed boundary conditions.

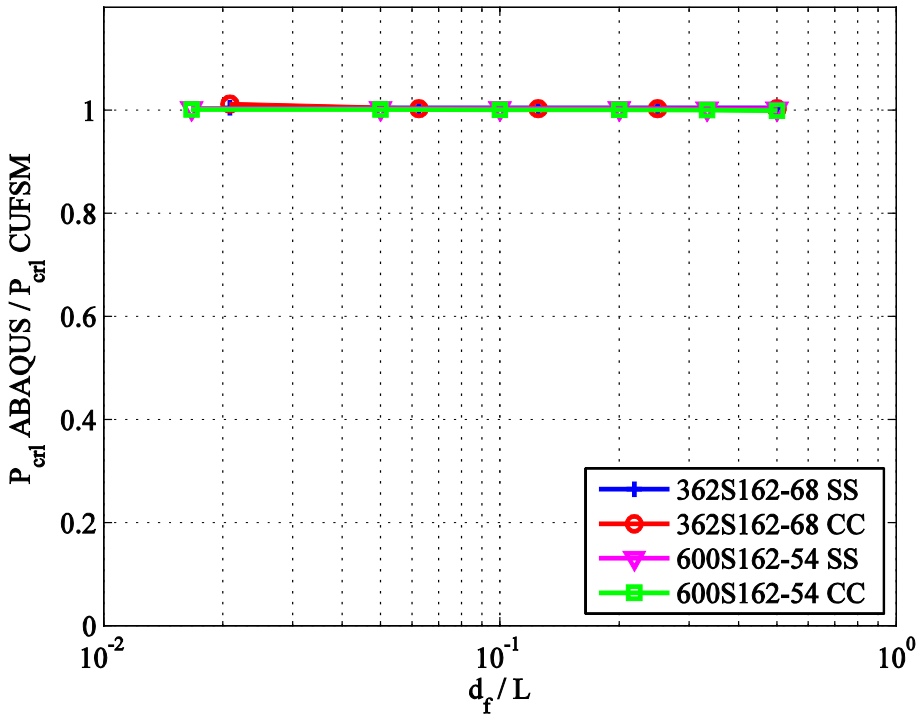

Figure 18 Plot of ratio of P_{cr} in ABAQUS to P_{cr} in CUFSM against ratio of fastener spacing to length (d_f/L) for local buckling.

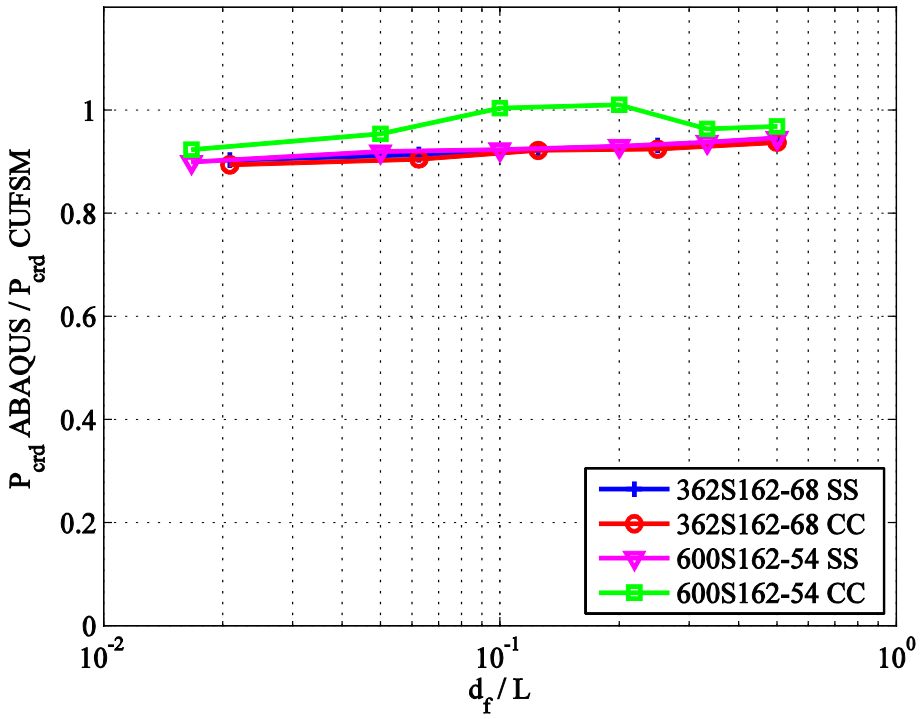

Figure 19 Plot of ratio of P_{cr} in ABAQUS to P_{cr} in CUFSM against ratio of fastener spacing to length (d_f/L) for distortional buckling.

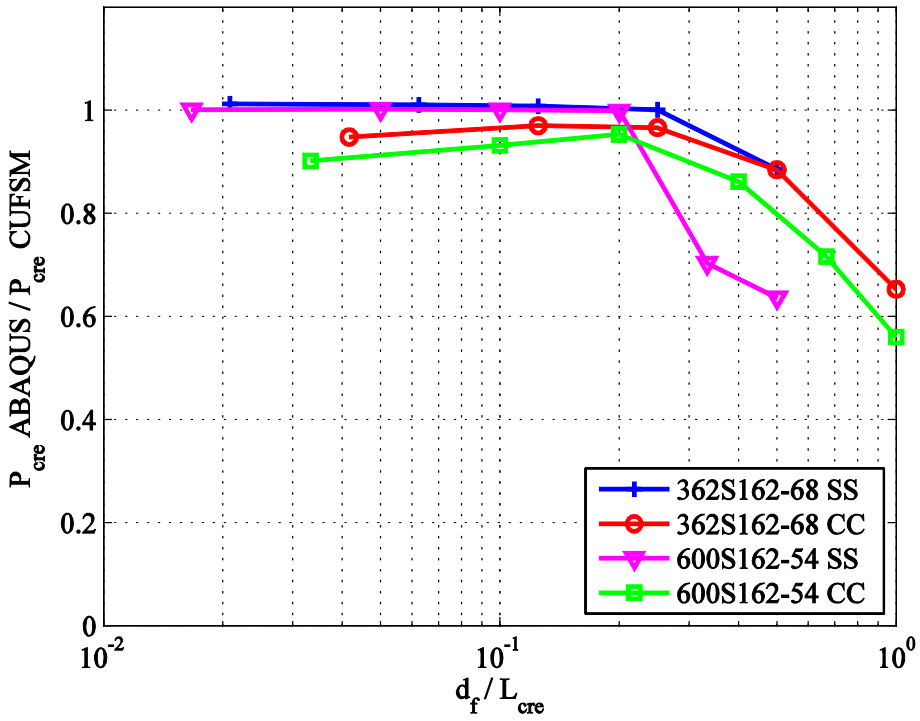

Figure 20 Plot of ratio of P_{cr} in ABAQUS to P_{cr} in CUFSM against ratio of fastener spacing to half-wavelength (d_f/L_{cre}) for global buckling.

Figure 18 reinforces that springs have no influence on local buckling, as the ratio of ABAQUS to CUFSM values remains approximately 1. Figure 19 shows that there is no obvious pattern of distortional buckling results with spring spacing. Also, the ratio of ABAQUS to CUFSM values is generally less than 1, which means that CUFSM values are greater. Figure 20 demonstrates that global buckling is influenced by springs the most. Also, plotting the critical loads against L_{cre} allows for the direct comparison of both simply-supported and fixed-fixed boundary conditions. The ratio of ABAQUS to CUFSM values appear to deviate from 1 when d_f/L_{cre} exceeds 0.25. Also, as is the case with distortional buckling, CUFSM values are almost always greater than ABAQUS values.

6.0 CONCLUSIONS

This parametric study provides a starting point for the comparison of smeared springs in CUFSM to discrete springs in ABAQUS. Two different cold-formed steel sections with different lengths were chosen for analysis. All other parameters were kept constant with only the fastener

spacing varying. The 96-inch 362S162-68 was chosen for direct comparison with Vieira (2011). The 120-inch 600S162-54, with a deeper cross-section, was chosen to best reflect the most common parameters selected in a survey. For both cases, it is apparent that spring spacing has no influence on local buckling and minimal influence on distortional buckling. However, springs play a significant role in providing restraint against global buckling. Based on the results, it can be concluded that the smeared spring assumption is only reasonable when $d_f/L_{cre} \leq 0.25$. Once that limit is exceeded, the smeared spring assumption should not be used. Also, the fact that CUFSM results were consistently greater than ABAQUS results means that CUFSM may be overstating P_{cr}, which could be problematic if this method is relied upon for design. A further investigation of boundary condition assumptions should be carried out to assure that both methods are as accurate as possible. Also, additional members and parameters should be analyzed to assure that the limit of $d_f/L_{cre} \leq 0.25$ is consistent.

REFERENCES

ABAQUS, *ABAQUS/CAE Version 6.9-1*, D. Systemes, Editor 2007.

AISI, Cold-Formed Steel Design Manual, American Iron and Steel Institute, 2008.

AISI-S100, North American Specification for the Design of Cold-Formed Steel Structural Members. American Iron and Steel Institute, 2007.

Li, Z., Schafer, B.W. "Application of the finite strip method in cold-formed steel member design." Journal of Constructional Steel Research, 2010. 66(8-9): p. 971-980.

Schafer, B.W., Ádány, S. "Buckling analysis of cold-formed steel members using CUFSM: conventional and constrained finite strip methods. "Eighteenth International Specialty Conference on Cold-Formed Steel Structures, Orlando, FL, October 2006.

SSMA, Product Technical Information, ICBO ER-4943P, S.S.M. Associations, Editor 2001.

Vieria, L.C.M. (2011). "Behavior and Design of Sheathed Cold-Formed Steel Stud Walls Under Compression," dissertation, presented to Johns Hopkins University at Baltimore, MD, in fulfillment of the requirements for the degree of Doctor of Philosophy.

APPENDIX A – *Results of Axial Load Bearing Sheathing-Based Design Stud Wall Survey*

Note: Histograms show number of professionals who voted for each parameter choice from a survey conducted at AISI-COS/COFS in February 2012.

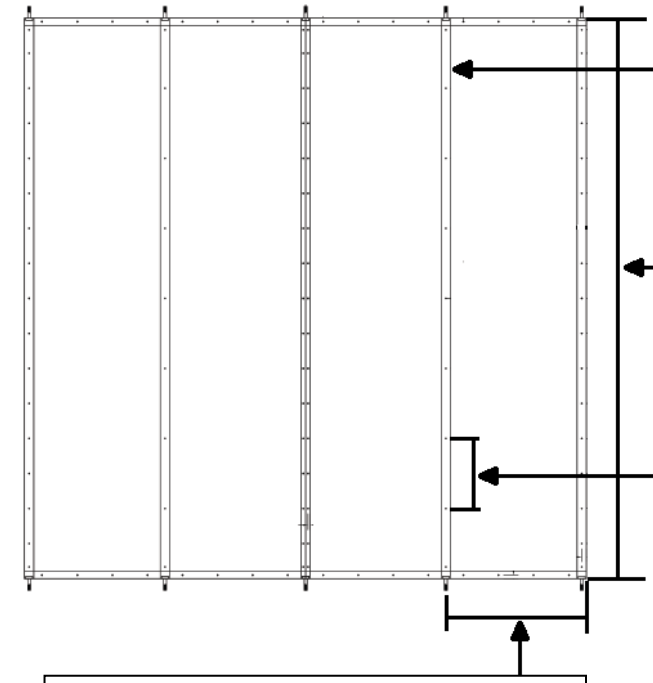

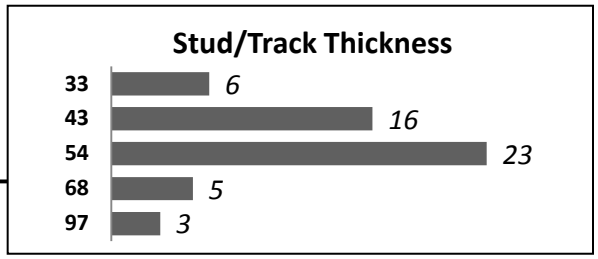

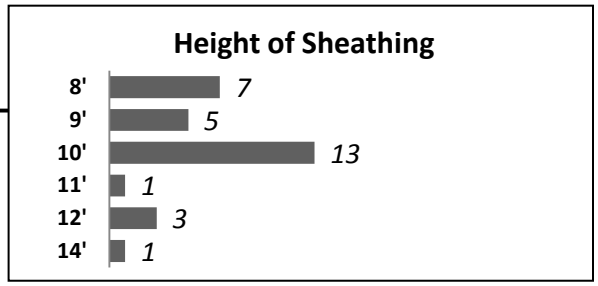

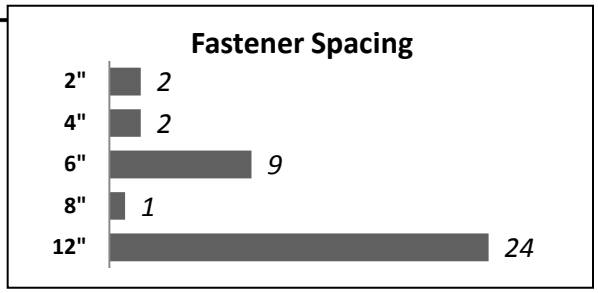

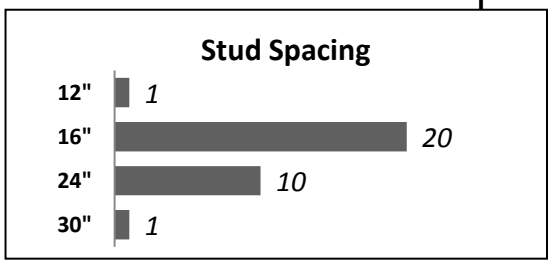

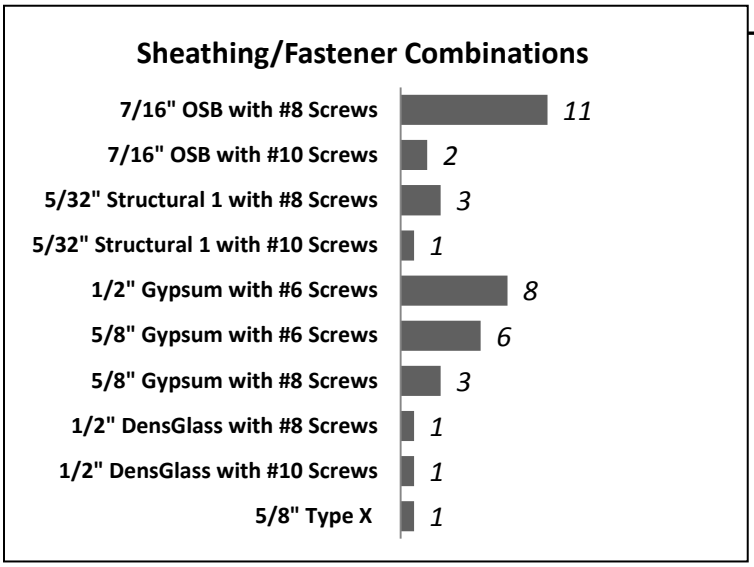

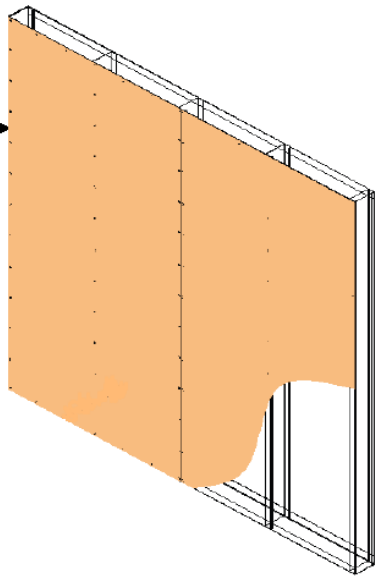

APPENDIX B – *Sample Spring Stiffness Calculations*

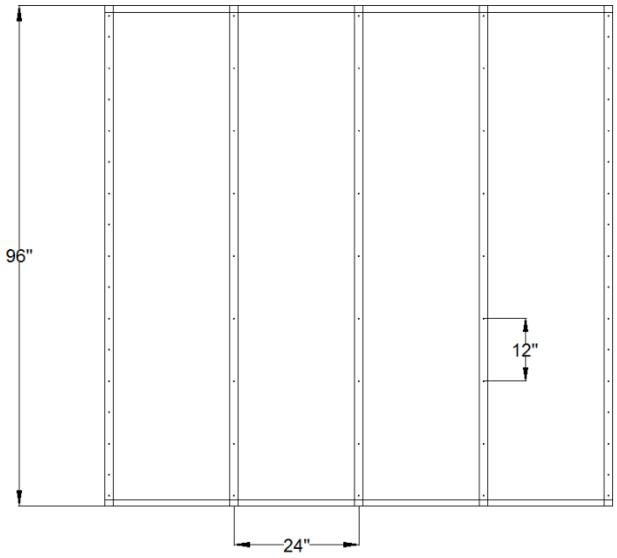

Cold-formed steel stud (362S162-98)

A = 0.524 in^2 (cross-sectional area)
E = 29,500 ksi (Young's modulus)
f_y = 50 ksi (yield strength)
t = 0.0713 in (thickness)

OSB sheathing (attached to both sides)

G = 190 ksi (shear stiffness)
t_{board} = 7/16 in (thickness)
L = 96 in (length)
$(EI)_{w\text{-}parallel}$ = 78 k-in^2/ft (sheathing rigidity, stress parallel to the strength axis)
$(EI)_{w\text{-}perpendicular}$ = 16 k-in^2/ft (sheathing rigidity, stress perpendicular to the strength axis)

Fasteners (#8)

d_f = 12 in (fastener spacing)
w_{tf} = 24 in (stud spacing)
d = 0.164 in (diameter of fastener)

Translational stiffness in the plane of the board (k_x)

k_{xd} = diaphragm stiffness

$$k_{xd} = \frac{\pi^2 G t_{board} d_f w_{tf}}{L^2} = \frac{\pi^2 (190ksi)(7/16in)(12in)(24in)}{(96in)^2} = 25.639 kips/in \quad (1)$$

$$\underline{k}_{xd} = \frac{k_{xd}}{d_f} = \frac{25.639 kips/in}{12in} = 2.136 kips/in/in$$

$k_{x\ell}$ = local stiffness

$$k_{x\ell} = \frac{3Ed^4t^3\pi}{4t_{board}^2(9d^4\pi + 16t_{board}t^3)} = \frac{3(29{,}500ksi)(0.164in)^4(0.0713in)^3\pi}{4(7/16in)^2(9*(0.164in)^4\pi + 16*(7/16in)(0.0713in)^3)} = 4.142kips/in \quad (2)$$

$$\underline{k}_{x\ell} = \frac{k_{x\ell}}{d_f} = \frac{4.142kips/in}{12in} = 0.345kips/in/in$$

k_x = overall stiffness

$$k_x = \left(\frac{1}{k_{x\ell}} + \frac{1}{k_{xd}}\right)^{-1} = \left(\frac{1}{4.142kips/in} + \frac{1}{25.639kips/in}\right)^{-1} = 3.57kips/in \quad (3)$$

$$\underline{k}_x = \frac{k_x}{d_f} = \frac{3.57kips/in}{12in} = 0.297kips/in/in \quad (4)$$

Translational stiffness out of the plane of the board (k_y)

$$(EI)_{w-parallel} = \frac{78k\cdot in^2}{ft} \times 2\,ft = 156kips$$

$$k_y = \frac{(EI)_{w-parallel}\pi^4 d_f}{L^4} = \frac{(156kips)\pi^4(12in)}{(96in)^4} = 0.00215kips/in \quad (5)$$

$$\underline{k}_y = \frac{k_y}{d_f} = \frac{0.00215kips/in}{12in} = 1.79\times10^{-4}kips/in/in \quad (6)$$

Rotational stiffness (k_ϕ)

$$(EI)_{w-perpendicular} = 16{,}000\frac{lb\cdot in^2}{ft} \times \frac{1ft}{12in} = 1{,}333.33\frac{lb\cdot in^2}{in}$$

$$\underline{k}_{\phi c} = 0.00035Et^2 + 75 = 0.00035*(29{,}500ksi)(0.0713)^2 + 75 = 127.5lb\cdot in/in/rad \quad (7)$$

$$\underline{k}_{\phi w} = \frac{(EI)_{w-perpendicular}}{d_f} = \frac{1{,}333.33lb\cdot in^2/in}{12in} = 111.1lb\cdot in/in/rad \quad (8)$$

$$\underline{k}_\phi = \frac{1}{\left(\frac{1}{k_{\phi c}} + \frac{1}{k_{\phi w}}\right)} = \frac{1}{\left(\frac{1}{127.5} + \frac{1}{111.1}\right)} = 59.37lb\cdot in/in/rad = 0.0594kips\cdot in/in/rad \quad (9)$$

$$k_\phi = \underline{k}_\phi \cdot d_f = (0.0594kip\cdot in/in/rad)(12in) = 0.712kips\cdot in/rad \quad (10)$$

APPENDIX C – *Spring Stiffness Values for Both CUFSM and ABAQUS*

Table C.1 Spring stiffness values for 362S162-68

	CUFSM			ABAQUS		
Spring Spacing (in)	$\underline{k}_x$ (kips/in/in)	$\underline{k}_y$ (kips/in/in)	$\underline{k}_\phi$ (kips-in/in/rad)	k_x (kips/in)	k_y (kips/in)	k_ϕ (kips-in/rad)
None	-	-	-	-	-	-
2	1.05	0.000179	0.107	2.10	0.000358	0.214
6	0.522	0.000179	0.081	3.13	0.00107	0.486
12	0.297	0.000179	0.0594	3.57	0.00215	0.712
24	0.160	0.000179	0.0387	3.83	0.00429	0.929
48	0.0829	0.000179	0.0228	3.98	0.00859	1.095

Table C.2 Spring stiffness values for 600S162-54

	CUFSM			ABAQUS		
Spring Spacing (in)	$\underline{k}_x$ (kips/in/in)	$\underline{k}_y$ (kips/in/in)	$\underline{k}_\phi$ (kips-in/in/rad)	k_x (kips/in)	k_y (kips/in)	k_ϕ (kips-in/rad)
None	-	-	-	-	-	-
2	0.498	0.0000489	0.093	0.995	0.0000977	0.186
6	0.261	0.0000489	0.0727	1.57	0.000293	0.436
12	0.152	0.0000489	0.0548	1.83	0.000586	0.657
24	0.083	0.0000489	0.0367	1.99	0.00117	0.881
40	0.0517	0.0000489	0.0255	2.07	0.00195	1.02
60	0.0351	0.0000489	0.0184	2.11	0.00293	1.11

APPENDIX D – *Sample Visual Comparison of ABAQUS and CUFSM for 362S162-68*

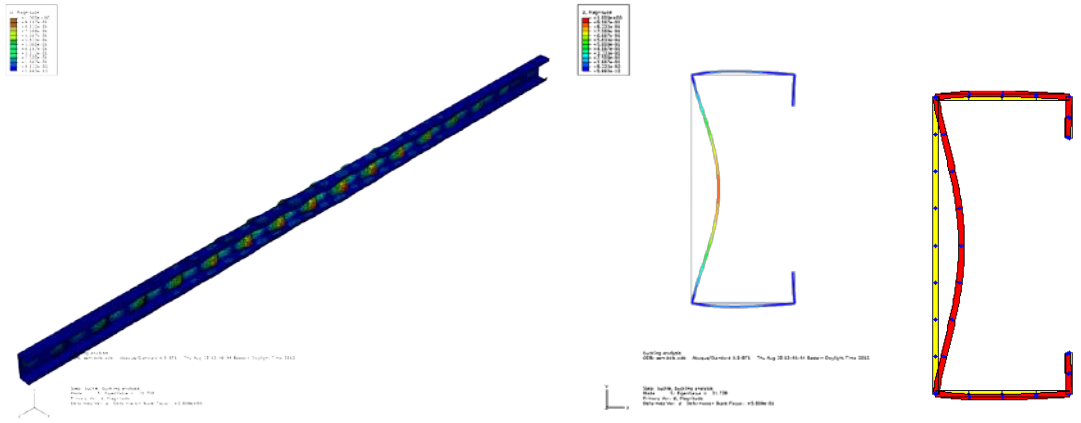

Figure D1 Local buckling of 362S162-68 with no springs and simply-supported boundary conditions at y/L=0.33.

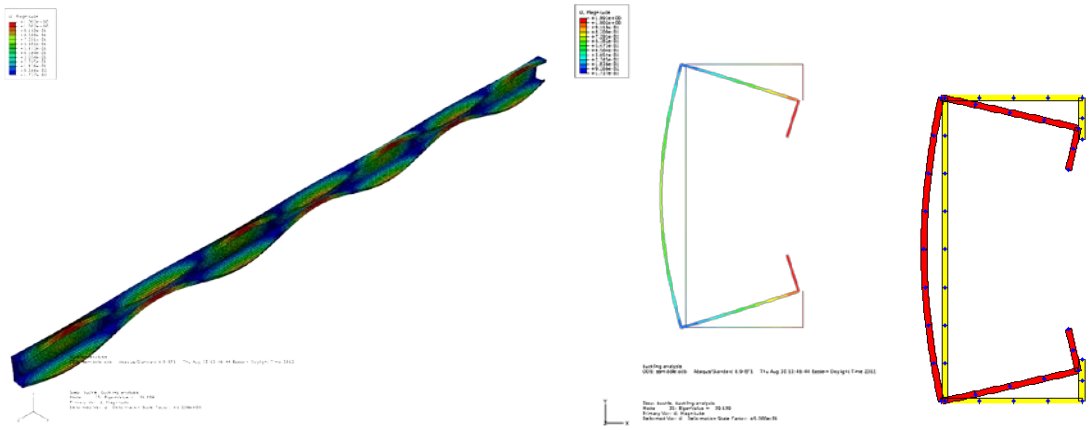

Figure D2 Distortional buckling of 362S162-68 with no springs and simply-supported boundary conditions at y/L=0.5.

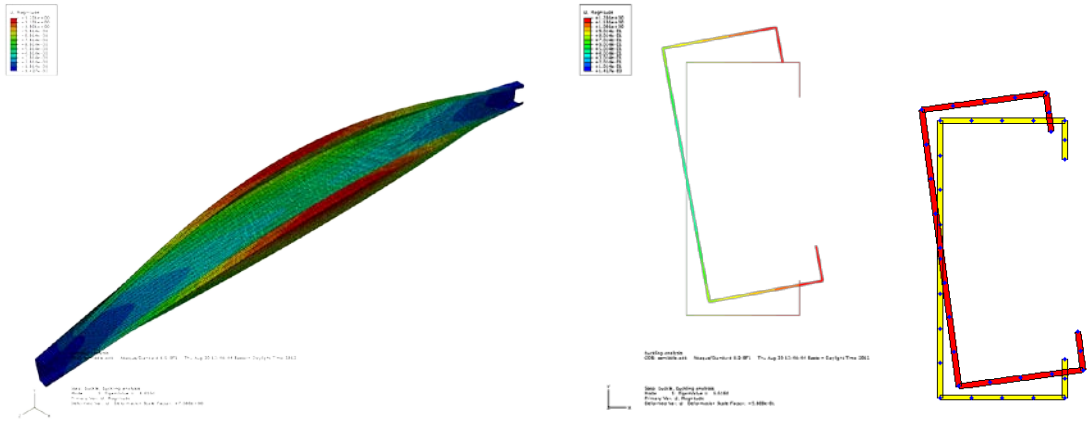

Figure D3 Global buckling of 362S162-68 with no springs and simply-supported boundary conditions at y/L=0.5.

APPENDIX E – *Sample Visual Comparison of ABAQUS and CUFSM for 600S162-54*

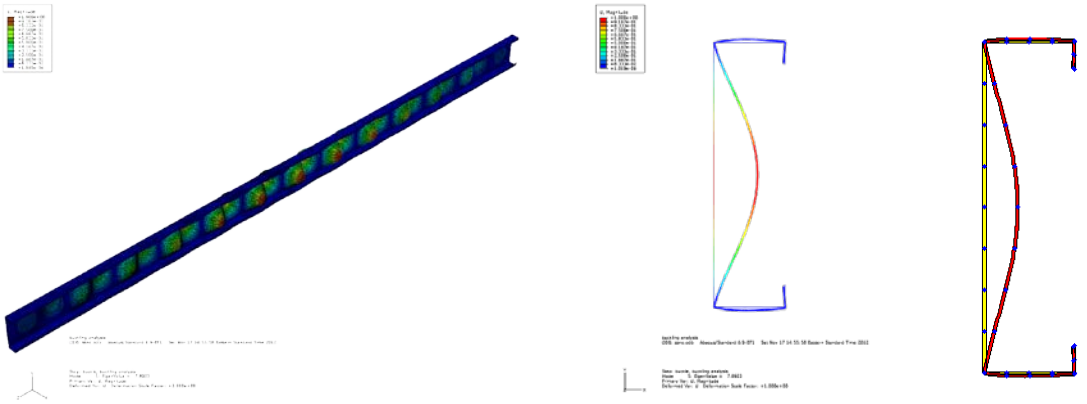

Figure E1 Local buckling of 600S162-54 with no springs and simply-supported boundary conditions at y/L=0.5.

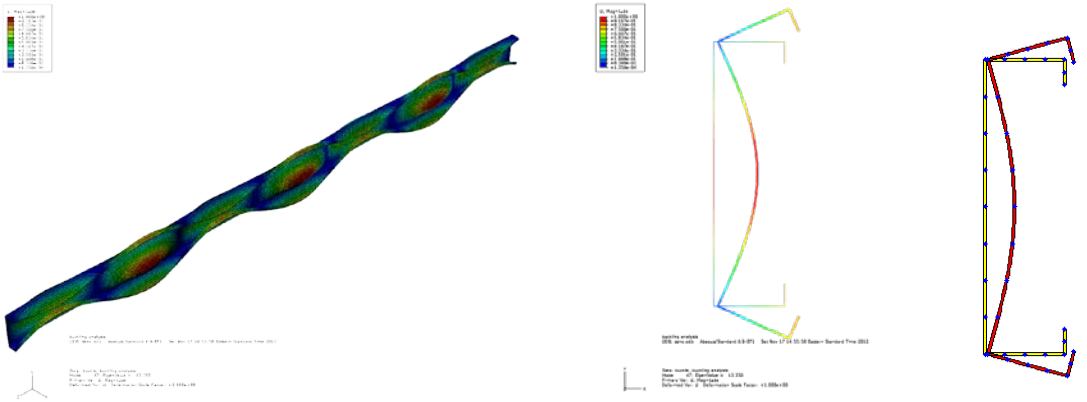

Figure E2 Distortional buckling of 600S162-54 with no springs and simply-supported boundary conditions at y/L=0.5.

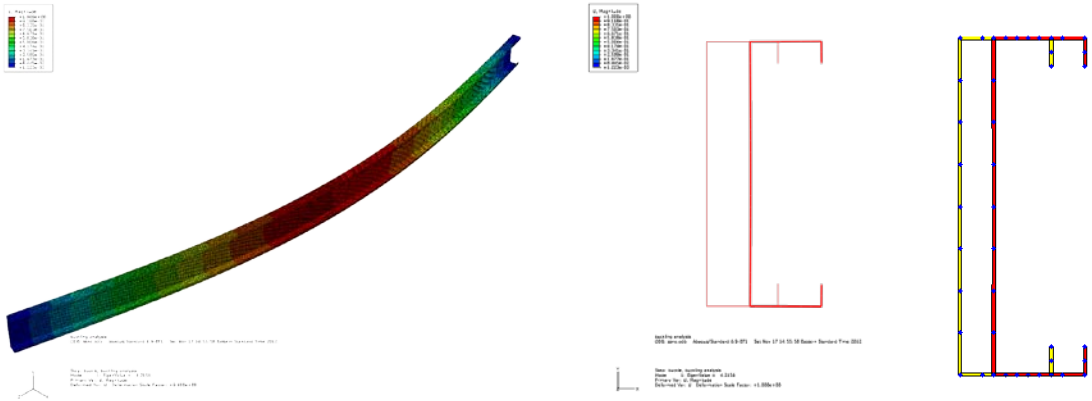

Figure E3 Global buckling of 600S162-54 with no springs and simply-supported boundary condition at y/L=0.5.